Preclinical Characterization of XL092, a Novel Receptor Tyrosine Kinase Inhibitor of MET, VEGFR2, AXL, and MER

Jeff Hsu, Colin Chong, Jeffrey Serrill, Levina Goon, Joan Balayan, Eric N. Johnson, Grachelle Lorenzana, Sharon Wu, Kevin G. Leong, Theodore J. Yun, Yong Wang, Faming Jiang, Lynne Bannen, Peter Lamb, Wei Xu, and Peiwen Yu

ABSTRACT

The multi-receptor tyrosine kinase inhibitor XL092 has been developed to inhibit the activity of oncogenic targets, including MET, VEGFR2, and the TAM family of kinases TYRO3, AXL and MER. Presented here is a preclinical evaluation of XL092. XL092 causes a significant decrease in tumor MET and AXL phosphorylation ($P < 0.01$) in murine Hs 746T xenograft models relative to vehicle, and a 96% inhibition of VEGFR2 phosphorylation in murine lungs. Dose-dependent tumor growth inhibition with XL092 was observed in various murine xenograft models, with dose-dependent tumor regression seen in the NCI-H441 model. Tumor growth inhibition was enhanced with the combination of XL092 with anti-PD-1, anti-programmed death ligand-1 (PD-L1), or anti-CTLA-4 compared with any of these agents alone in the MC38 murine syngeneic model and with anti-PD-1 in the CT26 colorectal cancer survival model. *In vivo*, XL092 promoted a decrease in the tumor microvasculature and significant increases of peripheral $CD4^+$ T cells and B cells and decreases in myeloid cells versus vehicle. Significant increases in $CD8^+$ T cells were also observed with XL092 plus anti-PD-1 or anti-PD-L1 versus vehicle. In addition, XL092 promoted M2 to M1 repolarization of macrophages *in vitro* and inhibited primary human macrophage efferocytosis in a dose-dependent manner. In summary, XL092 was shown to have significant antitumor and immunomodulatory activity in animal models both alone and in combination with immune checkpoint inhibitors, supporting its evaluation in clinical trials.

Introduction

MET, VEGFR2, and the TAM family of kinases (TYRO3, AXL, and MER) play important roles in tumorigenesis (1–10). MET and TAM kinases are widely expressed in numerous cancer types (1, 2), and are associated with the promotion of tumor angiogenesis and cancer cell growth, survival, invasion, and metastasis (1, 3, 4). VEGFR2 signaling stimulates endothelial cell proliferation and tumor angiogenesis, which facilitates tumor growth and metastasis (10). Because of the role of these kinases in tumor biology, a number of small-molecule inhibitors against these targets have been developed for the treatment of cancer, including the multi-receptor tyrosine kinase (RTK) inhibitor cabozantinib (11).

MET, VEGFR, and TAM kinases are also involved in immune cell modulation (1, 5, 6, 12–17). MET activation increases programmed death ligand-1 (PD-L1) expression on tumor cells and promotes immune-suppressive neutrophil mobilization (1, 12, 13). VEGFR activation promotes an immune-suppressive environment by increasing the activity of regulatory T cells and myeloid-derived suppressor cells, reducing tumor lymphocyte infiltration, and inhibiting the maturation of dendritic cells into antigen-presenting cells (APC; refs. 16, 17). The TAM kinases are broadly expressed on immune cell lineages within the tumor microenvironment, with their activation promoting an anti-inflammatory and immune-suppressive environment (5, 6). TAM kinase activation also decreases recruitment of cytotoxic T cells and tumor MHC class I expression (14, 15), polarizes macrophages toward an M2 anti-inflammatory phenotype (1), and promotes efferocytosis, the process by which apoptotic cellular material is internalized, thereby preventing an inflammatory response (9). Cabozantinib, an inhibitor of these kinases, has shown significant clinical activity when combined with immune checkpoint inhibitors (ICI; refs. 18–21).

XL092 is a novel small-molecule RTK inhibitor whose targets include MET, VEGFR2, and the TAM kinases TYRO3, AXL, and MER. Presented in this article is the preclinical characterization of XL092, including its ability to inhibit cellular RTK activity; reduce tumor growth *in vivo*, both alone and in combination with ICIs; inhibit angiogenesis; and promote an immune-permissive environment.

Materials and Methods

Compounds and reagents

XL092 (**Fig. 1A**) was synthesized at Exelixis and WuXi AppTec, as described in WO2019148044A1 (Compound # 8; ref. 22). For *in vitro* assays, 10 mmol/L XL092 was prepared from dry powder in sterile DMSO, dissolved by vortexing and sonicating, and serially diluted in the appropriate assay media, with the final DMSO concentration ≤ 0.4%. For *in vivo* studies, XL092 formulations were freshly prepared prior to dosing via oral gavage using 5%/45%/50% ETOH/PEG400/H_2O as a vehicle for most studies. For MDA-MB-231 xenograft studies, XL092 was formulated using Solutol (BASF).

Antibodies

For IHC, antibodies used were from Cell Signaling Technology for CD31 (#77699S) and for CD8 (#98941S). For

Exelixis, Inc., Alameda, California.

Corresponding Author: Peiwen Yu, Discovery Sciences & Technologies, Exelixis, Inc., 1851 Harbor Bay Parkway, Alameda, CA 94502. Phone: 650-837-7150; E-mail: pyu@exelixis.com

Mol Cancer Ther 2023;22:179–91

doi: 10.1158/1535-7163.MCT-22-0262

immunoprecipitation performed for Western blot analysis, antibodies used were from R&D Systems [Goat-anti-mouse antibody, VEGFR2 (#AF644) and AXL (#AF154)]. For Western blot analysis, antibodies used were from Cell Signaling Technology [VEGFR2 (#9698), pAXL (#5724), and cMET (#4560S)], Thermo Fisher Scientific [pVEGFR2 (#44-1047G) and pMET (#44-88G)] and Abcam [AXL (#ab215205)].

For flow cytometry, antibodies used for surface staining were: PD-L1 (MIH5; Thermo Fisher Scientific), PD-1 (29F.1A12; BioLegend), CD3 (145-2C11; BioLegend), CD11b (M1/70; BioLegend), CD45 (30-F11; BioLegend), CD8 (53-6.7; BioLegend), NKp46 (29A1.4; BioLegend), CD4 (RM4-5; BioLegend), Ly6G (1A8; BioLegend), CD11c (N418; Thermo Fisher Scientific), F4/80 (T45-2342; BD Biosciences), Ly6C (AL-21; BD Biosciences), MHC II (M5/114.15.2; BD Biosciences), CD19 (6D5; BioLegend), and CD25 (PC61; BioLegend). For intracellular staining, the antibodies used were: Arginase 1 (A1exF5; Thermo Fisher Scientific), Foxp3 (FJK-16s; eBioscience), Ki67 (Sola15; eBioscience), IFN (XMG1.2; BioLegend), and granzyme B (GB11; BioLegend).

Cell lines

Cell lines were purchased from ATCC (PC-3, Hs 746T, A-172, NCI-H441, SNU-5, CT26), Thermo Fisher Scientific (293A), AcceGen (MDA-MB-231), and NCI-DCTD Repository (MC38). Primary human umbilical vein endothelial cells (HUVEC) were purchased from Lonza.

For *in vitro* studies, human PC-3 (prostate), Hs 746T (gastric), A-172 (brain), NCI-H441 (lung), SNU-5 (gastric), and 293A (kidney) cell lines were passaged for less than 3 months and maintained in DMEM, containing 10% FBS, 1% penicillin-streptomycin, 1% nonessential amino acids, and 2 mmol/L GlutaMax (Gibco). The human MDA-MB-231 (breast) cell line was maintained in L-15 medium containing 10% FBS and 1% penicillin-streptomycin. The murine MC38 (colon) cell line was cultured in DMEM containing 10% FBS, 100 units/mL penicillin G sodium, 100 μg/mL streptomycin sulfate, 25 μg/mL gentamicin, and 2 mmol/L glutamine. All cells lines were incubated at 37°C in a humidified, 5% CO_2 atmosphere and grown until 80%–90% confluent for experiments. Primary HUVEC were passaged for less than 1 month and maintained in endothelial cell basal medium-2 (EBM-2, Lonza) containing supplements (EGM-2 BulletKit media, Lonza) and 1% penicillin-streptomycin. HUVEC were incubated at 37°C in a humidified, 5% CO_2 atmosphere and grown until 70%–80% confluent for experiments.

All cell lines used for *in vivo* studies were grown in tissue culture flasks in a humidified incubator (37°C, 5% CO_2). SNU-5 cells were maintained in Iscove's Modified Dulbecco's Medium (IMDM) containing 20% FBS, 0.15% sodium bicarbonate, 100 units/mL penicillin G sodium, 100 μg/mL streptomycin sulfate, 25 μg/mL gentamicin, and 2 mmol/L glutamine. Hs 746T cells were maintained in DMEM containing 10% FBS. MDA-MB-231 and NCI-H441 cells were maintained according to ATCC-recommended culture protocols in L-15 and RPMI1640, respectively, with 10% FBS. MC38 murine cells were cultured in DMEM containing 10% FBS, 100 units/mL penicillin G sodium, 100 μg/mL streptomycin sulfate, 25 μg/mL gentamicin, and 2 mmol/L glutamine. CT26 cells were cultured in RPMI1640 supplemented with 10% FBS. *In vitro* experiments were performed within 25 passages for cancer cell lines and eight passages for HUVEC after thawing, while *in vivo* studies were performed within four passages after thawing. All cells were confirmed to be *Mycoplasma* negative by PCR (IDEXX).

Kinase inhibition assays

Kinase activity inhibition with XL092 was investigated using the HTRF-KinEASE-TK assay platform from Cisbio. Reactions were performed in 384-well white, solid bottom, nonbinding surface plates. Compound was diluted in DMSO and then further diluted in buffer to maintain a constant percent DMSO in the kinase reaction. The assay was performed according to manufacturer's instructions with the exception that the enzyme was added last. The fluorescence resonance energy transfer reaction was allowed to incubate for 60 minutes at room temperature and emission at 620 and 665 nm was read on the PHERAstar FSX plate reader (BMG Labtech). ATP competition studies were conducted by determining IC_{50} values for XL092 using increasing ATP concentrations for MET, VEGFR2, AXL, and MER. Dose–response analysis was performed at ATP concentrations proximal to the K_m for the respective kinase. Nine to 11 different inhibitor concentrations were used in 384-well microtiter plate KinEASE experiments evaluating the function of each kinase.

Kinase profiling was performed using the ^{33}P-Phosphoryl transfer radiometric kinase assay by the KinaseProfiler service of Eurofins Pharma Discovery Services UK Limited (as described in KinaseProfiler Assay Protocol Guide Eurofins version 83.1). The KinaseProfiler assay measured kinase catalytic activity using recombinant proteins consisting of the active kinase domain. Dose–response experiments were performed using nine compound concentrations in a 96-well microtiter plate. For each assay, all compounds were prepared to a 50× final assay concentration (50 μmol/L) in 100% DMSO, then diluted in half-log series with the final top concentration at 1 μmol/L. This working stock of the compound was added to the assay well as the first component in the reaction, followed by the remaining components. The positive control wells (100% kinase activity) contained all components of the reaction including 2% DMSO (control for solvent effects), except for the compound of interest. Blank wells contained all components of the reaction, with the reference inhibitor, staurosporine. This reference compound was used to abolish kinase activity and generated the 0% kinase activity baseline.

Inhibition of receptor phosphorylation

Receptor phosphorylation of MET was assessed in both PC-3 and Hs 746T cells. Receptor phosphorylation of VEGFR2, AXL, MER, and TYRO3 was assessed in HUVEC and A-172, MERTK-transfected 293A (Genecopoeia, EX-Z8208-M02), and TYRO3-transfected 293A (Genecopoeia, EX-Z8208-M02) cells, respectively. Cells were serum-starved for 3–24 hours, incubated for 1 hour in serum-free medium with serially diluted XL092, and cells without constitutively active receptor were stimulated with human hepatocyte growth factor (PC-3), human Gas6 (A-172), or human VEGF165 (HUVEC). For MET assays in PC-3, cells were stimulated for 10 minutes with recombinant human hepatocyte growth factor (100 ng/mL, R&D Systems). For AXL assays in A-172, cells were stimulated for 15 minutes with recombinant human Gas6 (1 μg/mL, R&D Systems), and for VEGFR2 assays in HUVEC, cells were stimulated for 5 minutes with recombinant human VEGF165 (100 ng/mL, R&D Systems). Following treatment, cells were lysed with cold lysis buffer [20 mmol/L Tris, 137 mmol/L sodium chloride, 2 mmol/L Ethylenediaminetetraacetic acid, 10% glycerol, 1% NP-40 alternative, 1 mmol/L activated sodium orthovanadate, 1 mmol/L PefaBloc SC (Sigma-Aldrich), protease/phosphatase inhibitor tablet (Thermo Fisher Scientific)].

Lysates from stimulated cells, clarified by centrifugation, were analyzed in the PathScan phospho-Met (panTyr) Sandwich ELISA

(Cell Signaling Technology), the human phospho-AXL DuoSet IC ELISA (R&D Systems), the human phospho-VEGFR2 DuoSet IC ELISA (R&D Systems), the human phospho-MER DuoSet IC ELISA (R&D Systems), or the human phospho-TYRO3 ELISA (Cell Signaling Technology). Assays were performed according to manufacturer's instructions.

Cellular proliferation

Cells were grown in base medium (NCI-H441: RPMI1640; MDA-MB-231: L-15; SNU-5: IMDM; HUVEC: F-12K) + 10% FBS + 1% penicillin-streptomycin (complete media) at 5% CO_2 and 37°C. For the assay, cells were seeded (NCI-H441: 6,000 cells/well; MDA-MB-231: 5,000 cells/well; SNU-5: 7,500 cells/well; HUVEC: 1,500 cells/well) in 50 μL of the above complete media/well in triplicate, except for HUVEC cells which were plated in EGM2 BulletKit media (Lonza) containing VEGF among other endothelial growth supplements. Cells were plated in 384-well, black, clear bottom microplates (Corning) and incubated at 5% CO_2 and 37°C overnight. Cells were then treated with serial dilutions of XL092 and incubated for an additional 48 hours.

The Cell Proliferation ELISA, BrdU Chemiluminescent Kit (Sigma-Aldrich) was then used to analyze proliferation according to manufacturer's recommendations. Briefly, 10 μL of 0.5x BrdU labeling solution was added to each well and plates were incubated at 37°C for 2 hours. Labeling medium was then replaced with 75 μL of FixDenat solution and incubated at room temperature for 30 minutes. Medium was then removed by direct aspiration except for SNU-5 cell plates, where plates were spun at 300 × *g* for 10 minutes prior to medium removal. After fixation, the FixDenat solution was removed via vacuum aspiration and 30 μL anti-BrdU-POD working solution was added to each well, followed by incubation at room temperature for 90 minutes. FixDenat solution was removed following centrifugation, followed by the plates being washed 3× with 75 μL/well washing solution, allowing 5 minutes of incubation between washes. Following centrifugation and wash removal, 30 μL/well substrate solution was added to plates. Plates were read on the Perkin Elmer Envision Multimode Plate Reader and data were analyzed in ActivityBase version 9.5 (IBDS).

Immunoprecipitation and Western blot analysis of MET and AXL phosphorylation *in vivo*

Following euthanasia, SNU-5 and NCI-H441 tumors were harvested, minced, and resuspended in ice-cold radioimmunoprecipitation assay buffer containing protease/phosphatase inhibitors. Tumors were homogenized, centrifuged (14,000 rpm, 10 minutes, 4°C), and supernatants were stored at −80°C. Lysate protein concentrations were determined using the bicinchoninic acid method, pooled into 200 μg aliquots for each group, and incubated overnight at 4°C with rabbit anti-MET coupled to magnetic Sepharose-Protein A beads. Beads were then washed with lysis buffer, resuspended in 2x sample buffer, and boiled for 5 minutes at 95°C. Lysates were run on 4%–12% Bis-Tris gels, transferred to nitrocellulose membranes, blocked for 1 hour, and then incubated with primary antibodies for phospho- and total-MET overnight at 4°C. Membranes were then washed and incubated with corresponding secondary antibodies, and analyzed using an Odyssey CLx imager (LI-COR). Immunoblot signals were measured using LI-COR Image Studio software, and quantitation was determined by normalizing phosphorylation signals to total, nonphosphorylated signals and then calculating percent inhibition compared with vehicle-treated control signals. Hs 746T tumors were processed similarly, but lysates were additionally probed for AXL phosphorylation and quantified using Jess Western blot (Protein Simple).

VEGFR2 pharmacodynamic analysis

Hs 746T tumor-bearing mice were administered 10 μg of recombinant human VEGF (hVEGF) intravenously 3.5 hours after single oral doses of XL092 at 30 and 100 mg/kg or vehicle and 30 minutes prior to sacrifice. Lung tissue was harvested, homogenized, and immunoprecipitated overnight using an anti-VEGFR2 antibody coupled to magnetic Sepharose-Protein A beads. Western analysis was performed using primary antibodies for phospho- and total-VEGFR2 and corresponding secondary antibodies and analyzed using the Odyssey CLx imager (LI-COR), as described above.

In vivo xenograft and syngeneic tumor models

Six to 7 weeks old male NCr nu/nu mice were obtained from Beijing Vital River Laboratory Animal Technology Co., Ltd, and used for NCI-H441 pharmacodynamic and pharmacokinetic studies. Eight to 12 weeks old female CB.17-SCID mice were obtained from Charles River Laboratories and used for SNU-5 and Hs 746T xenograft studies. Six to 8 weeks old female NSG mice were obtained from Jackson Laboratories and used for MDA-MB-231 studies. Nine-week-old female C57BL/6 mice were obtained from Charles River Laboratories and used for MC38 syngeneic efficacy studies. Six to 8 weeks old female BALB/c mice were obtained from Charles River Laboratories and used for CT26 syngeneic efficacy studies.

The cell lines and tumor models selected were relevant to the main inhibitory targets of XL092, including those associated with high levels of MET activity or tumor angiogenesis via VEGFR2. These include NCI-H441 [expresses significant levels of phosphorylated MET (23)], SNU-5 [*MET* amplification with gains of gene copy number (24)], Hs 746T [*MET* amplification with gains of gene copy number (24) and a *MET* Δ exon 14 skipping mutation (25)], and MDA-MB-231 [tumor angiogenesis model (26)].

For inoculations, cell lines were trypsinized, washed, counted, and resuspended in cold PBS. Following rear-flank inoculations, body weights and tumor volume were measured at least twice weekly, with mice randomized prior to dosing once the mean tumor volume reached approximately 120 mm^3 for MDA-MB-231 inoculations, approximately 90 mm^3 for SNU-5, approximately 100 mm^3 for NCI-H441, approximately 110 mm^3 for MC38, approximately 200 mm^3 for Hs 746T, and approximately 90 mm^3 for CT26. All measurements were recorded using Studylog software version 4.2.

For the *in vivo* tumor phosphorylation studies in the NCI-H441 and SNU-5 xenograft models, mice received by oral gavage once daily XL092 (3 or 10 mg/kg) or vehicle for 14 days. For the *in vivo* tumor phosphorylation study in the Hs 746T xenograft model, mice were administered 10 μg of recombinant hVEGF (R&D Systems) intravenously 3.5 hours after single oral doses of XL092 at 30 and 100 mg/kg or vehicle and 30 minutes prior to sacrifice. hVEGF was reconstituted at 100 μg/mL in sterile PBS containing at least 0.1% human or bovine serum albumin. Lung tissue was evaluated for VEGFR2 phosphorylation and tumor tissue for MET and AXL phosphorylation. In a separate study using the Hs 746T xenograft model, mice were treated with a single oral dose of XL092 (up to 100 mg/kg) with plasma XL092 and tumor target phosphorylation measured after 4 hours, with the mice treated at the 100 mg/kg dose also evaluated every 12 hours up to 48 hours. For evaluating tumor target phosphorylation, mice received 10 μg of recombinant hVEGF

intravenously 30 minutes prior to sacrifice. For the *in vivo* models where antitumor activity of XL092 was assessed, mice received XL092 or vehicle by oral gavage once daily at doses ranging from 1 to 60 mg/kg, with doses and study time length dependent on the tumor model.

For XL092 and anti-PD-1 antibody combination studies, mice with syngeneic MC38 tumors were treated with XL092 (3 mg/kg, orally once a day), anti-PD-1 antibody (5 mg/kg, twice a week for 2 weeks, i.p.), XL092 plus anti-PD-1 antibody, or vehicle for 35 days. For XL092 and anti-PD-L1 antibody combination studies, mice with MC38 tumors were treated with XL092 (3 mg/kg, orally once a day), anti-PD-L1 antibody (5 mg/kg, twice a week for 2 weeks, i.p.), XL092 plus anti-PD-L1 antibody, or vehicle for 28 days. For XL092 and anti-CTL-associated antigen (CTLA)-4 antibody combination studies, mice with MC38 tumors were treated with XL092 (3 mg/kg, orally once a day), anti-CTLA-4 antibody (5 mg/kg, day 1; 2.5 mg/kg days 4 and 7; i.p.), XL092 plus anti-CTLA-4 antibody, or vehicle for 26 days. Doses used for XL092 and the ICIs in the combination studies were the same as their dosing used as single agents. Anti-PD-1 antibody (clone RMP1-14, Bio X Cell), anti-PD-L1 antibody (clone 10F.9G2, Bio X Cell), and anti-CTLA-4 antibody (clone 9H10, Bio X Cell) were diluted in sterile PBS prior to dosing (5 mg/kg).

In the CT26 syngeneic tumor model for Kaplan–Meier analysis of survival, mice were treated daily with XL092 (30 mg/kg, orally once a day) for 34 days, with or without anti-PD-1 antibody (10 mg/kg, every 3–4 days for 5 weeks i.p.), or vehicle. In this model, animals were sacrificed if tumor volumes reached 2,500 mm^3.

Tumor growth inhibition (TGI) was assessed using the formula $TGI = [(Vc_1 - Vc_0) - (Vt_1 - Vt_0)/(Vc_1 - Vc_0)] \times 100\%$; Vc_1 and Vt_1 are the mean tumor volumes of control and treated groups at time of tumor extraction, while Vc_0 and Vt_0 are the corresponding mean tumor volumes at the start of dosing.

Animal welfare and regulatory compliance

All animal studies detailed herein were conducted in compliance with relevant Institutional Animal Care and Use Committee procedures, adhered to current American Association for Accreditation of Laboratory Animal Care recommendations for animal care and use, and were approved by the Exelixis and selected contract research organizations' Institutional Animal Care and Use Committees.

Plasma protein binding analysis

Plasma protein binding was measured using rapid equilibrium dialysis against PBS buffer in triplicate at a compound concentration of 10 μmol/L and an incubation time of 16 hours.

Pharmacokinetic analysis

For drug exposure assessment, blood samples were obtained using lateral tail vein bleeds at specific timepoints following XL092 administration. Other tissues were collected and either snap-frozen in liquid nitrogen or fixed in 10% formalin. Measurements of XL092 concentrations in plasma samples were obtained using LC/MS-MS.

IHC

For IHC analysis of endothelial cell proliferation, MC38 tumor-bearing mice were treated for 5 days with XL092 at 3, 10, and 30 mg/kg orally once a day or vehicle. For IHC analysis of immune cell infiltration, MC38 tumor-bearing mice were treated with XL092 at 10 mg/kg orally once a day for 7 days, anti-PD-L1 at 5 mg/kg i.p. on days 1, 2, 4, 6, the combination of XL092 plus anti-PD-L1, or vehicle. One hour after the last dose, tumors were harvested, processed, and probed for the markers CD31 (endothelial cell proliferation) or CD8 (immune cell infiltration). Evenly distributed regions from individual tumors were chosen for quantification of IHC markers.

Ten regions of interest (ROI) per tumor were annotated using Qupath software by the pathologist. Necrotic areas within the tumor and peritumoral connective tissue were excluded. Each ROI was 0.5 μm^2. Vascular density was determined by number of vessels per 0.5 μm^2, which was manually counted by the pathologist. The mean vascular density of 10 ROIs was used in the analysis. Twelve tumors per treatment group were evaluated unless they were either too small or had extensive necrotic regions.

Flow cytometry

Five to 6 weeks old C57BL/6 female mice were inoculated subcutaneously with 1×10^6 syngeneic MC38 colon carcinoma cells. After tumors reached approximately 200 mm^3, mice were randomized into treatment groups and dosed orally with 10 or 30 mg/kg XL092 once a day, anti-PD-1 or anti-PD-L1 antibody (5 mg/kg, i.p., days 1, 2, 4, 6), or the combination of XL092 plus anti-PD-1 or anti-PD-L1 antibody for 7 days, or vehicle. Single-cell suspensions of mouse tumor and spleen were prepared with gentle mechanical disruption using a Tumor Dissociation kit and gentleMACS Dissociator (Miltenyi Biotec). Surface staining was performed with antibodies against PD-L1, PD-1, CD3, CD11b, CD45, CD8, NKp46, CD4, Ly6G, CD11c, F4/80, Ly6C, MHC II, CD19, and CD25. After surface staining, cells were either fixed and permeabilized with FoxP3/Transcription Factor Staining Buffer Set (eBiosciences) according to manufacturer's instructions and stained with antibodies against Foxp3, Ki67, IFNγ, and granzyme B or fixed and permeabilized with Intracellular Fixation/Permeabilization Buffer Set (eBiosciences) according to manufacturer's instructions and stained with antibody against Arginase 1. Live/dead cells were determined using BD Horizon Fixed Viability Stain 780 (#565388, BD Biosciences). Sample data were collected on a Cytek Northern Lights flow cytometer (Cytek Biosciences) and analyzed using FlowJo software version 10.6.

Macrophage repolarization

For the preparation of M2 macrophages, human $CD14^+$ monocytes (StemExpress) were differentiated into M2 macrophages by culturing 1.0×10^6 cells/mL in CellXVivo Human M2 Macrophage Differentiation Kit (R&D Systems) at 37°C in a humidified, 5% CO_2 atmosphere for 6 days according to the manufacturer's instructions. After differentiation, cells were washed once in fresh RPMI complete media containing 10% FBS, 1% penicillin-streptomycin, 1% nonessential amino acids, and 2 mmol/L GlutaMax, and cryopreserved at −80°C in RPMI complete media containing 5% of DMSO.

For the repolarization assay, frozen M2 macrophages were thawed and seeded at 2.0×10^5 cells/well in a 96-well tissue culture plates in CellXVivo Human M2 Macrophage Differentiation Medium (R&D Systems). XL092 at 2, 4, and 6 μmol/L concentrations were tested in triplicate for each donor to determine the dose response in this assay. XL092 was added to the cells, followed by incubation at 37°C in a humidified, 5% CO_2 atmosphere for 7 days, with medium refreshment and XL092 replenishment on day 4. For flow cytometric analysis of M1 versus M2 macrophages, macrophages were phenotypically characterized by staining the cells with anti-CD163 APC antibody (BioLegend, 333610) and 7-Amino Actinomycin D (7-AAD) Viability Staining Solution (BioLegend)

after Fc block (BD Biosciences). Percentages of CD163-positive (M2) and CD163-negative (M1) macrophages were derived from 7-AAD–negative cell populations, with forward and side light-scatter characteristics for viable single cells. For fold change determinations for macrophage repolarization, a total of 5 donors were assessed. M1/M2 ratio was calculated by dividing the percentage of viable CD163-negative (M1) cells by the percentage of viable CD163-positive (M2) cells. DMSO-treated group was used as a control to calculate the M1/M2 ratio fold change. Flow cytometry was performed using a Cytek Northern Lights flow cytometer (Cytek Biosciences) and data analysis was performed using FlowJo software.

Macrophage efferocytosis live cell imaging

M2 macrophages were thawed and seeded at 1.0×10^4 cells/well into 96-well plates for 24 hours in complete RPMI containing 25 ng/mL M-CSF. M2 macrophages were then treated with DMSO or XL092, serially diluted to produce a 10-point dose curve in triplicate, and incubated at 37°C overnight. Jurkat cells were treated with 1 μmol/L camptothecin (Sigma-Aldrich) overnight to induce apoptosis, labeled with pHrodo Red kit (Sartorius) according to manufacturer's instructions, and 5.0×10^4 cells were added to each well of treated macrophages. Four 10x images per well were captured using an IncuCyte S3 (Sartorius) every hour for 6 hours and efferocytosis was calculated by measuring total red signal and subtracting background autofluorescence following manufacturer's instructions.

Statistical analysis

For kinase assays using the HTRF-KinEASE-TK assay platform, Prism 8.0 (GraphPad) was used for curve fitting and to calculate IC_{50} values by nonlinear regression analysis. For this, the four-parameter equation: $Y = \text{Bottom} + (\text{Top-Bottom})/(1+10^{((\log IC_{50} - X)^* \text{HillSlope})})$ was used, where Y is the observed signal, X is the inhibitor concentration, top and bottom are the upper and lower plateaus in the units of the *Y* axis, and HillSlope describes the steepness of the family of curves. To evaluate the apparent K_i values for XL092, the IC_{50} values of XL092 were plotted as a function of ATP concentration. Using the Cheng and Prusoff equation (27), the *y* intercept of a linear regression of the data is an estimate of the apparent K_i. $K_i = IC_{50}/(1 + ([\text{ligand}]/K_D))$. For kinase profiling assays, IC_{50} values were calculated by nonlinear regression analysis using the sigmoidal dose–response (variable slope) curve fit on XLFit version 5.3 (IBDS).

For IC_{50} determinations for cellular phosphorylation assays, a range of 8 to 10 different XL092 concentrations was used to determine the IC_{50} values in multiple cell-based ELISAs. IC_{50} values were calculated by nonlinear regression analysis using a four-parameter logistic equation: $Y = \text{min} + (\text{max} - \text{min})/(1 + [10^{\log EC_{50}}/X]^N)$, where Y is the observed signal, X is the concentration of XL092, min is the assay background signal in presence of DMSO alone or a reference inhibitor compound, max is the signal in the presence of DMSO alone or growth factor + DMSO, IC_{50} is the concentration of XL092 at 50% inhibition, and *N* represents the empirical HillSlope as a measure of cooperativity where typically *N* should approximate unity. Curve fitting was performed using the Levenberg–Marquardt algorithm in ActivityBase version 9.5 (IDBS).

For *in vivo* tumor data, statistical significance was measured using nonparametric Mann–Whitney *U* test. For macrophage efferocytosis assays, AUC of total red fluorescence from 0 to 6 hours was calculated for each well in Prism 8.1 (GraphPad). IC_{50} values were calculated by nonlinear regression analysis using a four-parameter logistic curve fit in Prism 8.1.

Data availability

The data generated in this study are available within the article and its Supplementary Data.

Results

XL092 inhibits RTK activity and cell proliferation

The kinase inhibitory activity of XL092 against several RTK targets was evaluated in biochemical assays and in cellular models. In biochemical assays, XL092 potently inhibited MET, AXL, MER, and VEGFR2 (**Table 1**; Supplementary Table S1). In profiling a panel of 405 protein kinases at a single concentration of 1 μmol/L, XL092 exhibited ≥ 70% inhibition of additional RTKs and TKs (Supplementary Table S2). XL092 IC_{50} values of approximately 50 nmol/L and below were found for a representative panel of these sensitive kinases (Supplementary Table S3). No activity was observed against serine or threonine kinases.

XL092 was also shown to inhibit kinase activity and proliferation of tumor and normal cells grown under basal or growth factor–stimulated conditions. XL092 inhibited autophosphorylation of MET (PC-3 and Hs 746T cells), AXL (A-172 cells), VEGFR2 (HUVEC), MER (transfected 293A cells), and TYRO3 (transfected 293A cells) with IC_{50} values ranging from 1.6 nmol/L (VEGFR2) to 306 nmol/L

Table 1. XL092 inhibits human kinase enzymatic activity and cellular kinase activity.

		Cellular kinase activity inhibition	
Kinase	Kinase inhibition, $IC_{50} \pm$ SEM (nmol/L)	Cell line/ligand (*N*[a])	Cellular $IC_{50} \pm$ SD (nmol/L)
MET	3.0 ± 0.27	PC-3/HGF (382)	11.9 ± 1.55
		Hs 746T/none (10)	25.4 ± 1.32
VEGFR2	15.0 ± 0.95	HUVEC/VEGF165 (382)	1.57 ± 1.52
AXL	5.8 ± 0.38	A-172/GAS6 (218)	3.89 ± 1.61
MER	0.6 ± 0.054	293A/none (291)	6.01 ± 1.56
TYRO3	NA	293A/none (20)	306 ± 1.37

Note: For enzymatic assays, IC_{50} was evaluated at 10 μmol/L ATP. Cellular assays were conducted in serum-free conditions. For cellular assays, IC_{50} was determined by ELISA methods.

Abbreviations: HUVEC, human umbilical vein endothelial cell; NA, not available; SD, standard deviation; SEM, standard error of the mean.

[a]Number of experimental replicates.

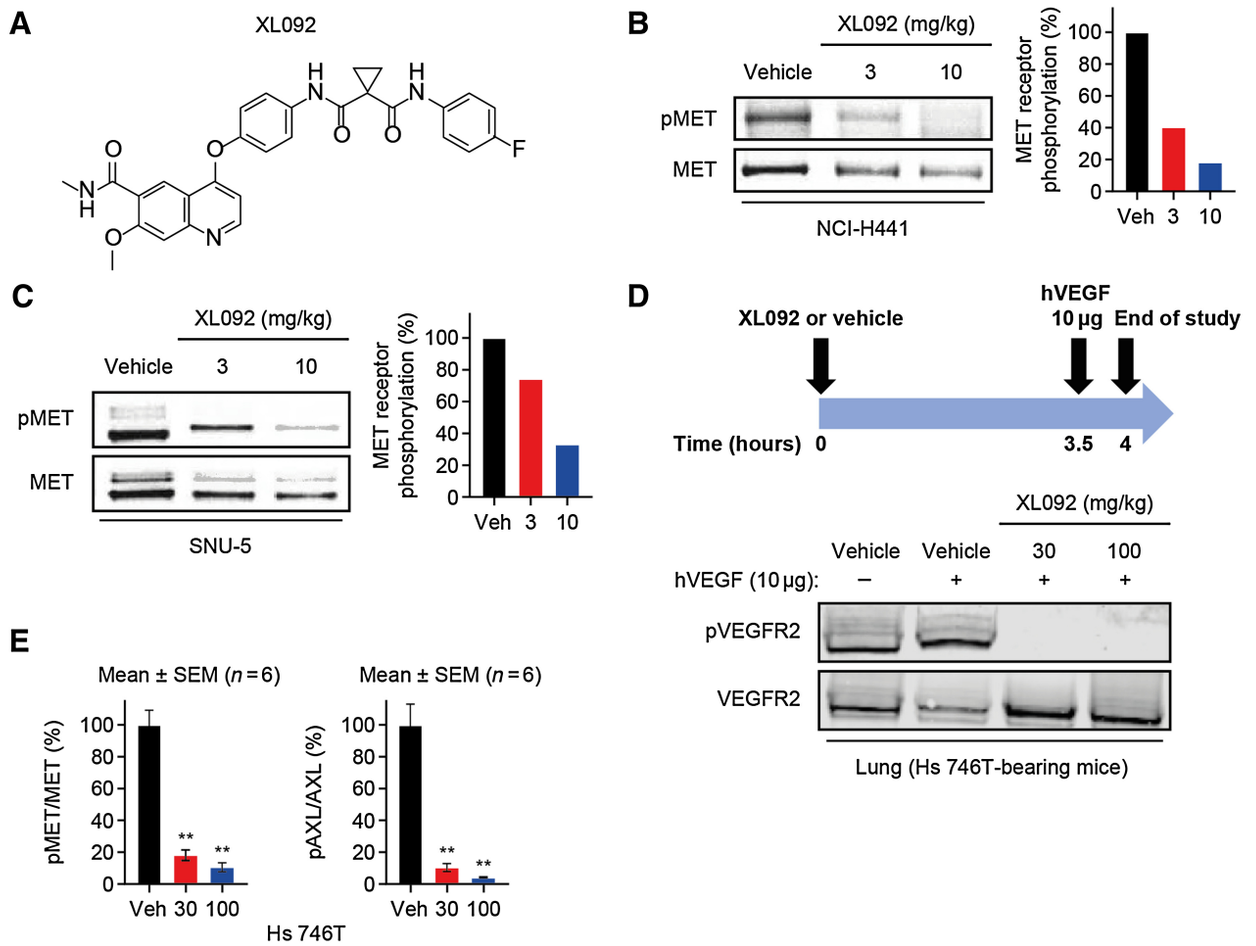

Figure 1.

XL092 inhibits MET, AXL, and VEGFR2 activation *in vivo*. **A,** Structure of XL092. pMET/MET levels were evaluated in NCI-H441 (**B**) and SNU-5 (**C**) tumors from mice treated with either 3 (red) or 10 (blue) mg/kg XL092 or vehicle (black) orally daily for 14 days ($n = 10$, pooled for each treatment group). **D,** pVEGFR2 and VEGFR2 levels were evaluated in hVEGF-treated Hs 746T tumor-bearing mouse lung tissue following single oral doses of 30 or 100 mg/kg XL092 ($n = 5$, pooled for each treatment group) or vehicle ($n = 6$, pooled). **E,** Mean pMET/MET and pAXL/AXL ratios ± SEM were measured in Hs 746T tumor-bearing mice treated with single oral doses of either 30 or 100 mg/kg XL092 or vehicle ($n = 6$ for each treatment group). Significance values were determined using a nonparametric Mann–Whitney *U* test with significance levels indicated using **, $P < 0.01$.

(TYRO3; **Table 1**). XL092 reduced the proliferation of several human tumor cell lines, including SNU-5 cells (IC_{50}, 98.9 nmol/L), which harbor an amplification of the MET gene (28), and HUVEC cells (IC_{50}, 10.4 nmol/L) (Supplementary Fig. S1).

XL092 inhibits MET, AXL, and VEGFR2 phosphorylation *in vivo*

The kinase inhibitory activity of XL092 was investigated in various murine xenogeneic tumor models and in mice lungs. Administration of XL092 to mice with NCI-H441 tumors caused a dose-dependent decrease in tumor MET phosphorylation (**Fig. 1B**). In this model, plasma concentrations of XL092 in the range of 2.4 to 9.7 µmol/L resulted in 60%–82% inhibition of MET phosphorylation (Supplementary Table S4). Mouse plasma protein binding for XL092 was 99.7%. Similarly, administration of XL092 caused a dose-dependent decrease in the phosphorylation of MET in SNU-5 tumors *in vivo* (**Fig. 1C**). Plasma concentrations of XL092 in the range of 1.9–7.6 µmol/L resulted in 26%–67% inhibition of MET phosphorylation in the SNU-5 xenografts (Supplementary Table S4).

Inhibition of VEGFR2 activation in lung tissue (a tissue with significant levels of VEGFR2) was observed in Hs 746T tumor-bearing mice, with complete abolishment of pVEGFR2 at 30 mg/kg (**Fig. 1D**). XL092 was also found to robustly inhibit the phosphorylation of MET and AXL in Hs 746T tumors (**Fig. 1E**). Plasma concentrations of XL092 were 20 and 63 µmol/L for the 30 and 100 mg/kg once a day doses (Supplementary Table S4), respectively. This inhibition of MET, AXL, and VEGFR2 phosphorylation was observed with XL092 4 hours after dose (Supplementary Fig. S2A). Furthermore, the inhibition of phosphorylation of these kinases in this model after a single dose of 100 mg/kg XL092 lasted for approximately 24 hours (Supplementary Fig. S2B).

XL092 inhibits tumor growth *in vivo* in a dose-dependent manner

The potency of XL092 in reducing tumor growth was evaluated in four different human xenograft murine models using the NCI-H441, Hs 746T, SNU-5, and MDA-MB-231 cell lines. Daily XL092 dosing

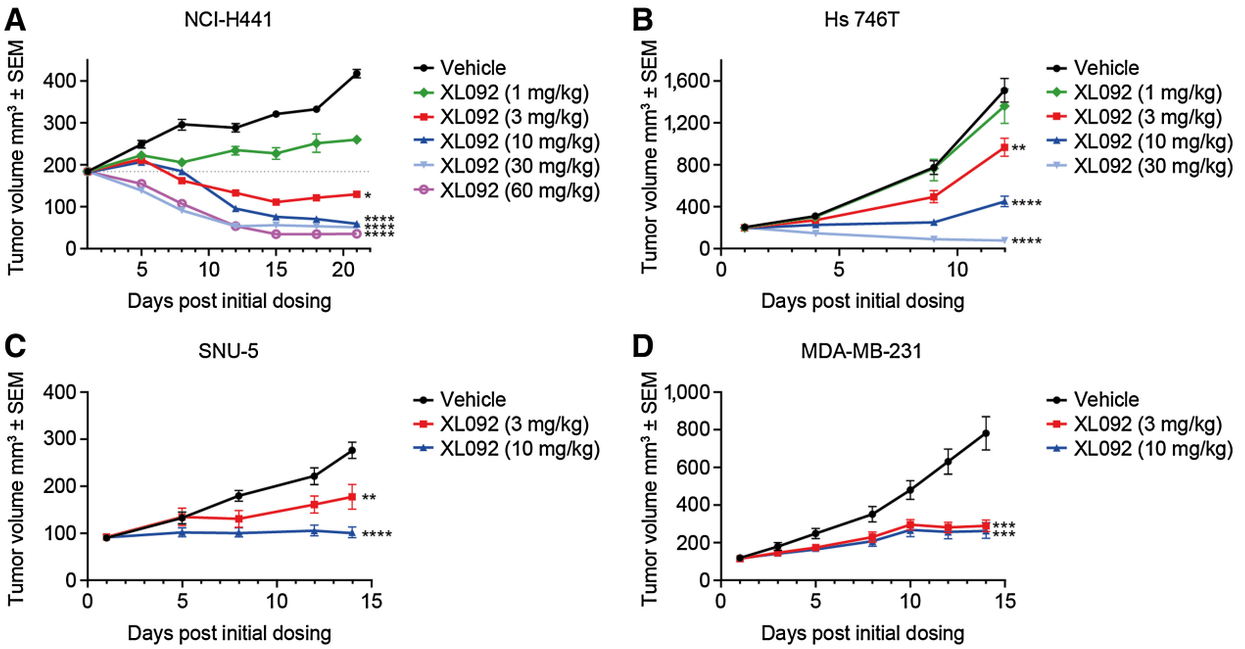

Figure 2.

XL092 exhibits antitumor activity in multiple xenograft models. Tumor-bearing mice NCI-H441 (**A**), Hs 746T (**B**), SNU-5 (**C**), and MDA-MB-231 (**D**) were dosed with XL092 or vehicle orally once daily as indicated in **Table 2**. Mean tumor volume ± SEM ($n = 10$) presented. Significance values represent % TGI levels, and were determined using a nonparametric Mann–Whitney *U* test, with significance levels indicated using *, $P < 0.05$; **, $P < 0.01$; ***, $P < 0.001$; ****, $P < 0.0001$.

resulted in significant TGI with dose dependency seen for the NCI-H441, Hs 746T, and SNU-5 tumor models (**Fig. 2**; **Table 2**). For the NCI-H441 tumor model, dose-dependent tumor regression was also observed. For all models, plasma concentrations of XL092 generally increased proportionally with increasing doses. Mouse plasma protein binding for XL092 was 99.7%. Analyses of plasma exposure samples from SNU-5 xenograft-bearing animals indicated a 94.7% TGI when XL092 reached a concentration of approximately 7.6 μmol/L at 4 hours after dose after 14 days of dosing. No significant body weight loss or adverse effects were observed with treatment (Supplementary Fig. S3A–S3D).

Table 2. TGI and XL092 dose exposure across four xenograft models.

Tumor model	Dose (mg/kg/day), duration (days)	Tumor growth inhibition	Tumor regression (%)	*P*
NCI-H441	1, 21	68.3	–	–
NCI-H441	3, 21	–	5.6	0.0115
NCI-H441	10, 21	–	67.7	<0.0001
NCI-H441	30, 21	–	72.1	<0.0001
NCI-H441	60, 21	–	86.1	<0.0001
Hs 746T	1, 12	10.1	–	–
Hs 746T	3, 12	35.6	–	0.0015
Hs 746T	10, 12	70.2	–	<0.0001
Hs 746T	30, 12	94.9	–	<0.0001
SNU-5	3, 14	54.2	–	0.0052
SNU-5	10, 14	94.7	–	<0.0001
MDA-MB-231	3, 14	73.6	–	0.0003
MDA-MB-231	10, 14	78.6	–	0.0002

Enhanced TGI with XL092 in combination with ICIs

XL092 was evaluated in combination with anti-PD-1, anti-PD-L1, or anti-CTLA-4 treatment in the MC38 murine syngeneic model (**Fig. 3**). Single-agent treatment with XL092 and anti-PD-1 resulted in significant TGI compared with vehicle, with greater inhibition observed with XL092 plus anti-PD-1 (**Fig. 3A**). Similar results were observed for the combination of XL092 plus anti-PD-L1 (**Fig. 3B**) and XL092 plus anti-CTLA-4 (**Fig. 3C**). No significant body weight loss or adverse effects were observed with treatment (Supplementary Fig. S3E–S3G)

In the less-sensitive CT26 colorectal cancer survival model, greater survival was observed for XL092 plus anti-PD-1 than for either of the single agents alone (Supplementary Fig. S4). The majority of mice that received the combination treatment (90% for 30 mg/kg XL092 and anti-PD-1 combination) survived to the end of the 34-day dosing regimen. In comparison, survival was markedly lower for the single-agent treatments (20% for 30 mg/kg XL092 and 50% for anti-PD-1). No adverse effects or significant weight loss were observed in any of the treatment groups throughout the duration of these experiments.

XL092 disrupts tumor vasculature

The antiangiogenic activity of XL092 was evaluated in a MC38 murine tumor model. Visually, a decrease in the number of blood vessels throughout the tumors was observed with XL092 treatment versus vehicle, and quantification indicated a decrease in tumor microvasculature after 7 days of treatment (**Fig. 4**).

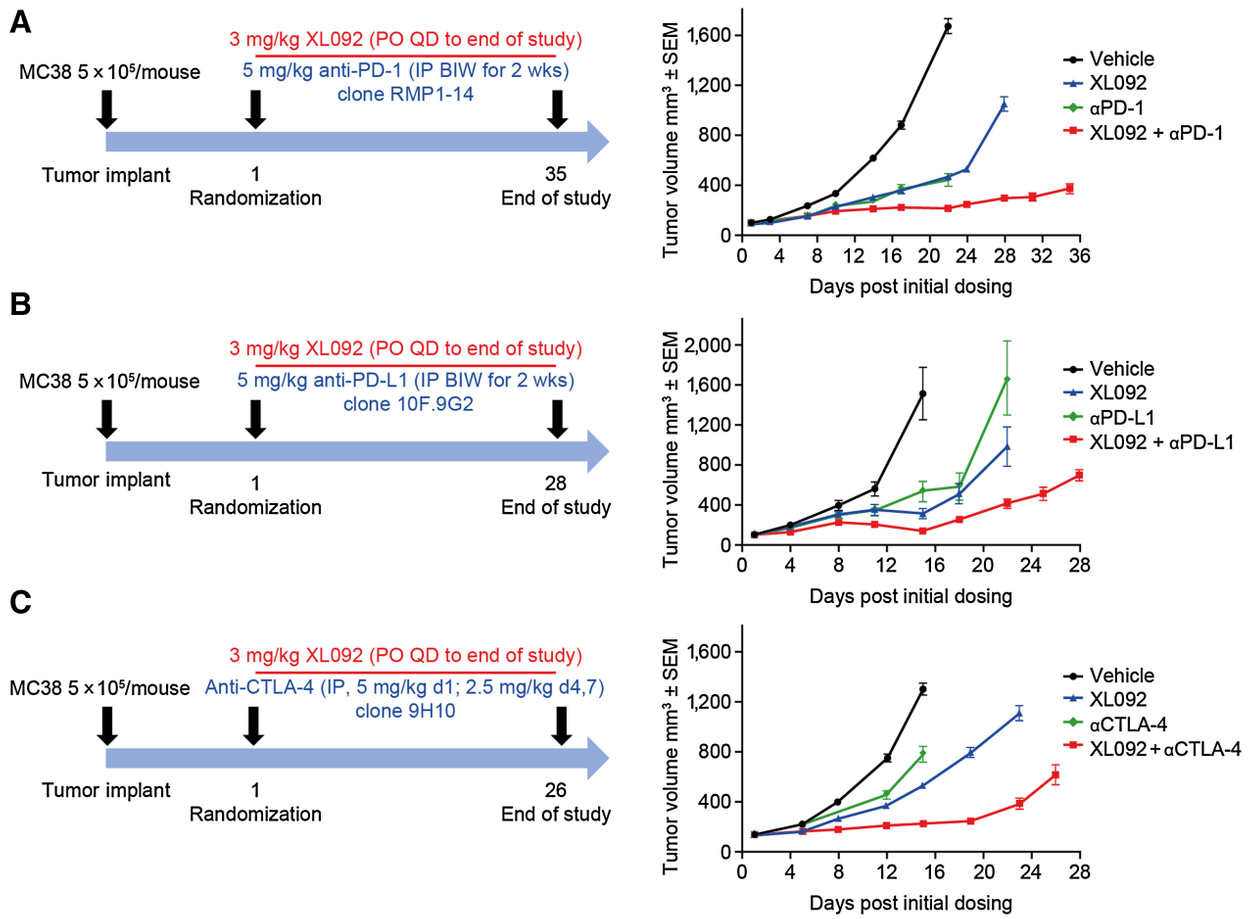

Figure 3.

Enhanced activity of XL092 plus ICI compared with single agents in MC38 syngeneic tumor model. Study design and tumor growth results in MC38 tumor-bearing mice treated with XL092 alone and in combination with ICI: anti-PD-1 (**A**), anti-PD-L1 (**B**), anti-CTLA-4 (**C**). Symbols represent mean tumor volume ± SEM ($n = 10$). BIW, twice a week. IP, intraperitoneal. PO, oral. QD, once a day.

XL092 treatment of MC38 syngeneic tumor-bearing mice is associated with a conversion to an immune-permissive tumor microenvironment

Because of the enhanced tumor growth inhibitory activity of the combination therapy, we explored potential underlying immunomodulating mechanisms of XL092. With XL092 there was a dose-dependent increase in peripheral $CD4^+$ T cells and B cells and a dose-dependent decrease in myeloid cells after 7 days of treatment in the MC38 syngeneic tumor model (**Fig. 5A**). At 30 mg/kg XL092, significant increases in peripheral $CD4^+$ T cells ($P < 0.05$) and B cells ($P < 0.0001$) and significant decreases in peripheral myeloid cells ($P < 0.0001$) relative to vehicle were noted. With either 5 mg/kg anti-PD-1 or anti-PD-L1 antibody, significant increases in peripheral B cells ($P < 0.01$) and decreases in peripheral myeloid cells ($P < 0.01$) relative to vehicle were observed (**Fig. 5A**). No significant increase in $CD8^+$ T cells was found with the single agents. Although similar findings as with XL092 were seen with the combination of 30 mg/kg XL092 plus either anti-PD-1 or anti-PD-L1 antibody, of note these combinations also resulted in significant increases in peripheral $CD8^+$ T cells ($P < 0.05$) relative to vehicle. Changes in tumor $CD8^+$ T-cell infiltration was also evaluated with an increase in tumor $CD8^+$ T cells observed with the combination of XL092 (10 mg/kg) plus anti-PD-1 antibody (5 mg/kg) but not with the individual agents (**Fig. 5B**).

XL092 repolarizes primary human macrophages from an M2 immune-suppressive to an M1 immune-permissive phenotype and inhibits primary human macrophage efferocytosis

The effect of XL092 on macrophage repolarization from an M2 to an M1 phenotype was evaluated. Dose-responsive effects of XL092 on repolarization of macrophages from an M2 to an M1 phenotype were observed in primary human $CD14^+$ monocyte-derived M2 macrophages (Supplementary Fig. S5). XL092 downregulated CD163 expression in M2 macrophages from 5 independent donors, resulting in dose-dependent increases in the M1 (CD163-negative) to M2 (CD163-positive) ratio.

Primary human macrophage efferocytosis of apoptotic Jurkat cells with XL092 was evaluated. In a dose-dependent manner, XL092 inhibited efferocytosis in primary human macrophages derived from 5 independent donors (IC_{50} range, 43–181 nmol/L; Supplementary Table S5).

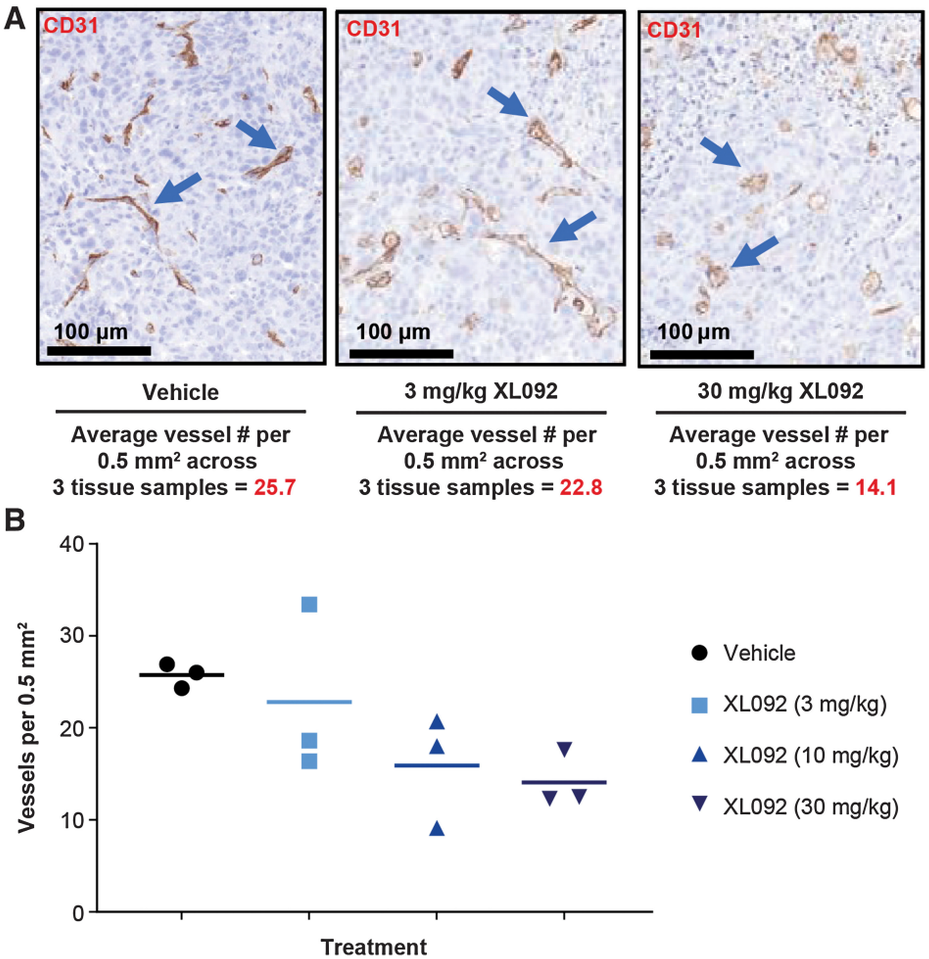

Figure 4.
Preliminary evaluation of XL092 effect on tumor angiogenesis *in vivo.* MC38 tumor-bearing mice were treated with a range of XL092 doses (orally, once a day) for 5 days, and tumors were analyzed for the presence of tumor microvessels by CD31 staining. **A,** Paraffin-embedded tumor tissue stained with the blood vessel marker CD31 (blue arrows). **B,** Density score of blood vessels across conditions. Horizontal bars represent mean values for $n = 3$ tumors per condition.

Discussion

XL092 demonstrated potent inhibition of MET, AXL, MER, and VEGFR2. Robust inhibition of these kinases by XL092 was also observed in various human cell lines and in various human tumor xenograft models in mice.

Dose-dependent TGI by XL092 was also demonstrated using several different murine xenograft or syngeneic models of human breast, gastric, lung, and colon cancer, with TGI reaching ≥ 70% after 14 days of daily 10 mg/kg treatments. Importantly, XL092 plasma concentrations corresponded well with the inhibition of MET, AXL, and VEGFR2 activity and tumor growth.

The potential for combination treatment of XL092 with ICI therapy was evaluated utilizing the MC38 syngeneic tumor model. Combination treatment of XL092 plus anti-PD-1, anti PD-L1, or anti-CTLA-4 antibody resulted in greater TGI compared with any of these agents alone. Combination treatment of XL092 plus anti-PD-1 in the CT26 tumor model also resulted in improved survival over time, with the percentage of mice alive at the end of the experiment greater than that of single-agent treatment. Throughout these studies, no decreases in body weight or other signs of overt toxicity were observed, suggesting that XL092 was tolerable in preclinical mouse models.

In addition to kinase inhibition, potential mechanisms were identified for TGI with XL092 and enhanced growth inhibition when used in combination with ICIs, including the promotion of an immune-permissive tumor environment and inhibition of angiogenesis. Given the high degree of expression of TAM kinases on a wide range of immune cell subtypes that promote tumor immunity, including T cells, natural killer cells, macrophages, myeloid-derived suppressor cells, and dendritic cells, the inhibition of their activity is of great interest for fostering an immune-permissive tumor microenvironment (6, 29, 30). XL092 treatment *in vivo* resulted in significant increases in peripheral $CD4^+$ T cells and B cells and significant decreases in peripheral myeloid cells. These changes were enhanced in combination with either anti-PD-1 or anti-PD-L1, along with the significant increase in peripheral $CD8^+$ T cells, which was not observed upon single-agent treatment with XL092 or the ICIs. Furthermore, increased tumor accumulation of $CD8^+$ T cells was observed with the combination of XL092 plus anti-PD-1.

XL092 also induced a dose-dependent repolarization of macrophages from the M2 anti-inflammatory phenotype toward the proinflammatory M1 phenotype, as well as a dose-dependent inhibition of macrophage efferocytosis activity *in vitro*. Repolarization of macrophages toward an M1 phenotype and inhibition of macrophage efferocytosis have both been identified as potential strategies for

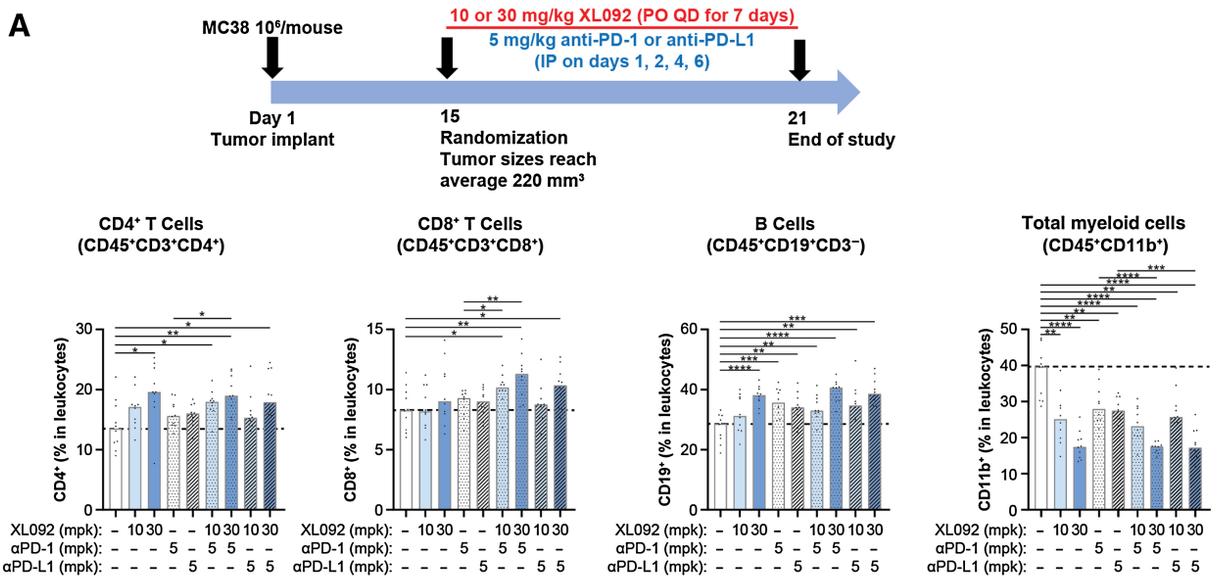
A
MC38 10⁶/mouse
10 or 30 mg/kg XL092 (PO QD for 7 days)
5 mg/kg anti-PD-1 or anti-PD-L1
(IP on days 1, 2, 4, 6)
Day 1
Tumor implant
15
Randomization
Tumor sizes reach
average 220 mm³
21
End of study
CD4⁺ T Cells
(CD45⁺CD3⁺CD4⁺)
CD8⁺ T Cells
(CD45⁺CD3⁺CD8⁺)
B Cells
(CD45⁺CD19⁺CD3⁻)
Total myeloid cells
(CD45⁺CD11b⁺)
CD4⁺ (% in leukocytes)
CD8⁺ (% in leukocytes)
CD19⁺ (% in leukocytes)
CD11b⁺ (% in leukocytes)
XL092 (mpk): – 10 30 – – 10 30 10 30
αPD-1 (mpk): – – – 5 – 5 5 – –
αPD-L1 (mpk): – – – – 5 – – 5 5

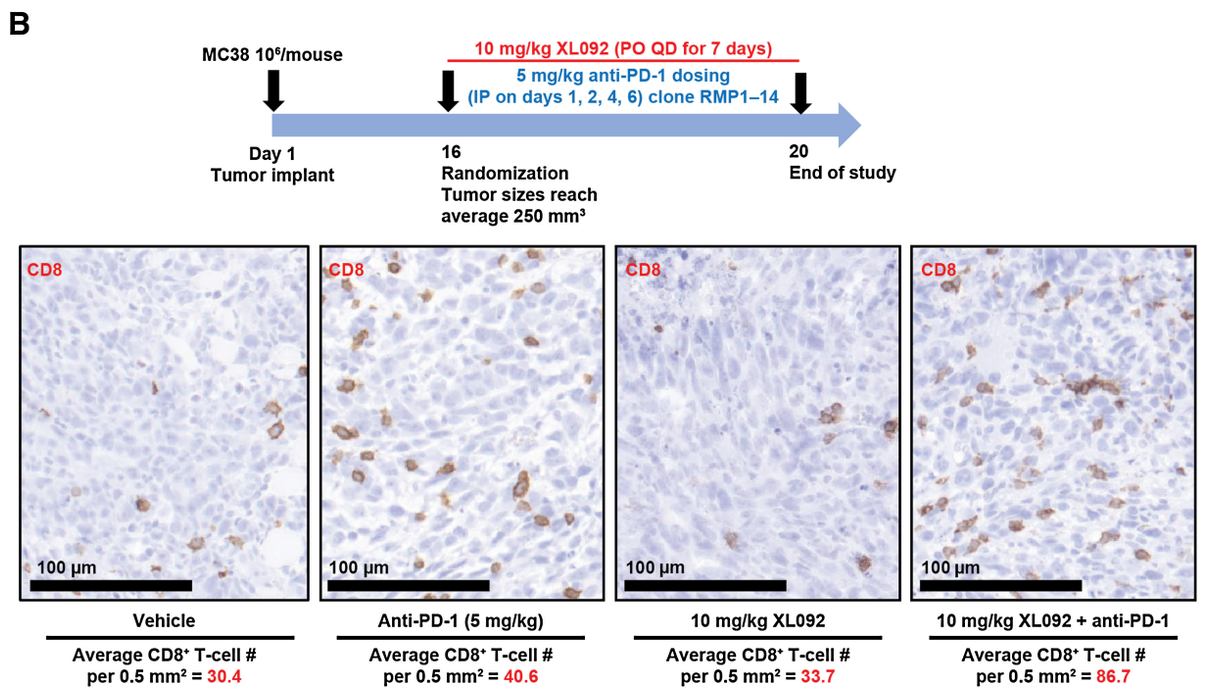
B
MC38 10⁶/mouse
10 mg/kg XL092 (PO QD for 7 days)
5 mg/kg anti-PD-1 dosing
(IP on days 1, 2, 4, 6) clone RMP1–14
Day 1
Tumor implant
16
Randomization
Tumor sizes reach
average 250 mm³
20
End of study
CD8
100 µm
Vehicle
Average CD8⁺ T-cell #
per 0.5 mm² = 30.4
Anti-PD-1 (5 mg/kg)
Average CD8⁺ T-cell #
per 0.5 mm² = 40.6
10 mg/kg XL092
Average CD8⁺ T-cell #
per 0.5 mm² = 33.7
10 mg/kg XL092 + anti-PD-1
Average CD8⁺ T-cell #
per 0.5 mm² = 86.7

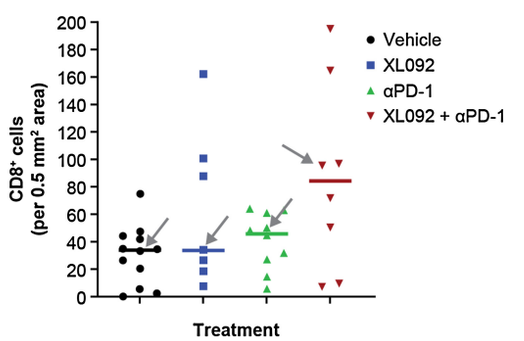
CD8⁺ cells
(per 0.5 mm² area)
Treatment
Vehicle
XL092
αPD-1
XL092 + αPD-1

targeting macrophage activities associated with tumor growth and survival (31, 32).

Both the MET and VEGFR signaling pathways are dysregulated in many tumor types, resulting in enhanced tumor angiogenesis and tumor cell proliferation and invasion (33, 34). By targeting multiple and redundant pathways involved in tumor growth and/or angiogenesis, including VEGFR, MET, and AXL, XL092 may provide multi-modal and complementary antitumor activity. A decrease in tumor vessel density was observed following exposure to XL092, although the sample size was small. The activity of VEGFR2, an integral mediator of both normal and tumor blood vessel formation, was also shown to be greatly inhibited with XL092.

XL092 has a kinase inhibitory profile that overlaps with cabozantinib, an RTK inhibitor with significant clinical activity as a single agent in a variety of tumors (35–39) and when combined with ICIs (18–21). Cabozantinib has a manageable safety profile but a relatively long plasma half-life of approximately 99 hours that results in drug accumulation during initial dosing and extends the washout period on cessation of dosing, which may complicate adverse event management (40). For XL092, preliminary pharmacokinetic data from an ongoing phase I trial (NCT03845166) reported a relatively short half-life of approximately 24 hours in humans to support once daily dosing (41), and a study in rats reported a half-life of approximately 7 hours (22).

Supplemental studies are needed to help further inform the clinical development of XL092, including direct comparisons of XL092 to cabozantinib with regard to target profile, pharmacokinetics, and pharmacodynamics, as well as activity in specific tumor types. Studies also should aim to further delineate the effects of XL092 on specific immune cell subsets and whether these effects contribute differently to the antitumor response when used in ICI-combination regimens in various cancer types. Supplemental studies are also needed to more fully characterize the antiangiogenic activity of XL092. Consideration should be given to the role tumor-associated macrophages have in the angiogenic process and hence tumor growth and survival. Tumor-associated macrophages produce a number of proangiogenic factors, such as VEGFA, placental growth factor, TNF, IL6, IL1β, CXCL8, and FGF 2 (42–44). By targeting TAM kinases, VEGFR, and MET signaling activity, decreasing efferocytosis, and shifting macrophages to an M1 polarization state, XL092 may consequently reduce the macrophage-associated role in angiogenesis. Future studies should also evaluate the immunomodulatory activity of XL092 with respect to VEGFR and MET.

In summary, XL092 is a novel RTK inhibitor which potently inhibits MET, AXL, MER, and VEGFR2; and has significant antitumor activity in animal models both alone and in combination with ICIs. In this preclinical evaluation, XL092 was shown to reduce angiogenesis and tumor cell proliferation and survival, and to promote an immune-permissive tumor microenvironment, including the repolarization of macrophages from an M2 immune-suppressive to an M1 immune-permissive phenotype and the inhibition of efferocytosis. These findings support the continued evaluation of XL092 in clinical studies.

Authors' Disclosures

All authors were employees of Exelixis Inc. at the time the work was performed. T.J. Yun reports other support from Exelixis, Inc outside the submitted work. Y. Wang reports a patent for WO2019148044 pending, a patent for WO2021222673 pending, and a patent for WO2021062245 pending. F. Jiang reports a patent for WO2019148044 issued and a patent for WO2019148043 issued. L. Bannen reports a patent for WO2019148044A1 pending. P. Lamb is an employee of and stockholder in Exelixis Inc. W. Xu reports a patent for WO2019148044A1 pending. No additional disclosures were reported by the other authors.

Authors' Contributions

J. Hsu: Conceptualization, data curation, formal analysis, supervision, investigation, visualization, methodology, writing–original draft, project administration, writing–review and editing, validation. **C. Chong:** Data curation, formal analysis, validation, investigation, visualization, methodology. **J. Serrill:** Conceptualization, data curation, formal analysis, validation, visualization, methodology, writing–original draft, writing–review and editing. **L. Goon:** Conceptualization, resources, data curation, formal analysis, supervision, validation, investigation, visualization, methodology, project administration. **J. Balayan:** Data curation, investigation, visualization, methodology. **E.N. Johnson:** Conceptualization, resources, data curation, formal analysis, supervision, validation, methodology, project administration. **G. Lorenzana:** Data curation, formal analysis, validation, investigation, methodology. **S. Wu:** Data curation, formal analysis, validation, investigation, visualization, methodology. **K.G. Leong:** Conceptualization, resources, data curation, formal analysis, supervision, validation, visualization, methodology, project administration, writing–review and editing. **T.J. Yun:** Conceptualization, resources, data curation, formal analysis, supervision, validation, visualization, methodology, project administration. **Y. Wang:** Conceptualization, data curation, formal analysis, validation, investigation, methodology. **F. Jiang:** Conceptualization, data curation, formal analysis, validation, investigation, methodology. **L. Bannen:** Conceptualization, resources, supervision, validation, visualization, project administration. **P. Lamb:** Conceptualization, resources, supervision, validation, visualization, project administration. **W. Xu:** Conceptualization, resources, supervision, validation, visualization, project administration. **P. Yu:** Conceptualization, resources, supervision, validation, visualization, project administration.

Acknowledgments

The authors would like to thank Jimmy Lai, Orville Cortez, Andy Wong, and Zoia Levashova for their contributions to data generation and discussion. Alonso Mariscal, Vincent Gloria, and Madeleine Brasch contributed to XL092 compound management and quality assurance. Linh Nguyen, Kevin Quinn, and Peter Haroldsen also contributed to ongoing clinical discussions and interpretation. Contributions were also made by Sylvie Privat (pharmacodynamic readout and immunophenotyping); David Santos (pharmacodynamic readout); Rizlane Nghima-Tahiri, Dhara Amin, and Raju Pusapati (immunophenotyping); Keith Yu and Christopher Chow (cellular assays); Nicholas Manieri (macrophage efferocytosis); Madelena Nguyen (biochemical and cellular assays, pharmacodynamic readout, and immunophenotyping); and

Figure 5.

Effect of XL092/ICI combination treatment on peripheral immunocytes and CD8 T-cell tumor infiltration. **A,** The proportion of peripheral leukocytes that were $CD4^+$ T cells, $CD8^+$ T cells, B cells, and total myeloid cells were determined in MC38 tumor-bearing mice treated for 7 days with XL092 (10 or 30 mg/kg), 5 mg/kg anti-PD-1 antibody, 5 mg/kg anti-PD-L1 antibody, XL092 plus either anti-PD-1 or anti-PD-L1 antibody, or vehicle. Presented are study design and results. Bars represent median with significance determined using a nonparametric Mann–Whitney *U* test, with significance levels indicated using *, $P < 0.05$; **, $P < 0.01$; ***, $P < 0.001$; ****, $P < 0.0001$. **B,** Changes in $CD8^+$ T-cell tumor density in MC38 tumor-bearing mice treated for 7 days with 10 mg/kg XL092 ($n = 7$), 5 mg/kg anti-PD-1 antibody ($n = 10$), XL092 plus anti-PD-1 antibody ($n = 8$) or vehicle ($n = 12$). Bars representing the mean displayed in the graph with arrows pointing to specific tumors representing the mean $CD8^+$ T-cell numbers in the figure. IP, intraperitoneal. mpk, mg per kg. PO, oral. QD, once a day.

Andrew Standeven (kinase profiling IC_{50}s). David Markby and Michael Raffin and Alan Saltzman (Fishawack Communications Inc. part of Fishawack Health) contributed to scientific writing and editorial assistance.

This study was supported by Exelixis, Inc.

The publication costs of this article were defrayed in part by the payment of publication fees. Therefore, and solely to indicate this fact, this article is hereby marked "advertisement" in accordance with 18 USC section 1734.

Note

Supplementary data for this article are available at Molecular Cancer Therapeutics Online (http://mct.aacrjournals.org/).

Received April 11, 2022; revised June 28, 2022; accepted November 10, 2022; published first November 18, 2022.

References

1. Graham DK, DeRyckere D, Davies KD, Earp HS. The TAM family: phosphatidylserine sensing receptor tyrosine kinases gone awry in cancer. Nat Rev Cancer 2014;14:769–85.
2. Gherardi E, Birchmeier W, Birchmeier C, Vande Woude G. Targeting MET in cancer: rationale and progress. Nat Rev Cancer 2012;12:89–103.
3. Rong S, Segal S, Anver M, Resau JH, Vande Woude GF. Invasiveness and metastasis of NIH 3T3 cells induced by Met-hepatocyte growth factor/scatter factor autocrine stimulation. Proc Natl Acad Sci U S A 1994;91:4731–5.
4. Michieli P, Mazzone M, Basilico C, Cavassa S, Sottile A, Naldini L, et al. Targeting the tumor and its microenvironment by a dual-function decoy Met receptor. Cancer Cell 2004;6:61–73.
5. Peeters MJW, Rahbech A, Thor Straten P. TAM-ing T cells in the tumor microenvironment: implications for TAM receptor targeting. Cancer Immunol Immunother 2020;69:237–44.
6. Akalu YT, Rothlin CV, Ghosh S. TAM receptor tyrosine kinases as emerging targets of innate immune checkpoint blockade for cancer therapy. Immunol Rev 2017;276:165–77.
7. Filardy AA, Pires DR, Nunes MP, Takiya CM, Freire-de-Lima CG, Ribeiro-Gomes FL, et al. Proinflammatory clearance of apoptotic neutrophils induces an IL-12(low)IL-10(high) regulatory phenotype in macrophages. J Immunol 2010;185:2044–50.
8. Fadok VA, Bratton DL, Konowal A, Freed PW, Westcott JY, Henson PM. Macrophages that have ingested apoptotic cells in vitro inhibit proinflammatory cytokine production through autocrine/paracrine mechanisms involving TGF-beta, PGE2, and PAF. J Clin Invest 1998;101:890–8.
9. Scott RS, McMahon EJ, Pop SM, Reap EA, Caricchio R, Cohen PL, et al. Phagocytosis and clearance of apoptotic cells is mediated by MER. Nature 2001;411:207–11.
10. Amini A, Masoumi Moghaddam S, Morris DL, Pourgholami MH. The critical role of vascular endothelial growth factor in tumor angiogenesis. Curr Cancer Drug Targets 2012;12:23–43.
11. Yakes FM, Chen J, Tan J, Yamaguchi K, Shi Y, Yu P, et al. Cabozantinib (XL184), a novel MET and VEGFR2 inhibitor, simultaneously suppresses metastasis, angiogenesis, and tumor growth. Mol Cancer Ther 2011;10:2298–308.
12. Balan M, Mier y Teran E, Waaga-Gasser AM, Gasser M, Choueiri TK, Freeman G, et al. Novel roles of c-Met in the survival of renal cancer cells through the regulation of HO-1 and PD-L1 expression. J Biol Chem 2015;290:8110–20.
13. Glodde N, Bald T, van den Boorn-Konijnenberg D, Nakamura K, O'Donnell JS, Szczepanski S, et al. Reactive neutrophil responses dependent on the receptor tyrosine kinase c-MET limit cancer immunotherapy. Immunity 2017;47:789–802.
14. Aguilera TA, Rafat M, Castellini L, Shehade H, Kariolis MS, Hui AB, et al. Reprogramming the immunological microenvironment through radiation and targeting Axl. Nat Commun 2016;7:13898.
15. Paolino M, Penninger JM. The role of TAM family receptors in immune cell function: implications for cancer therapy. Cancers 2016;8:97.
16. Ott PA, Hodi FS, Buchbinder EI. Inhibition of immune checkpoints and vascular endothelial growth factor as combination therapy for metastatic melanoma: an overview of rationale, preclinical evidence, and initial clinical data. Front Oncol 2015;5:202.
17. Voron T, Marcheteau E, Pernot S, Colussi O, Tartour E, Taieb J, et al. Control of the immune response by pro-angiogenic factors. Front Oncol 2014;4:70.
18. Bergerot P, Lamb P, Wang E, Pal SK. Cabozantinib in combination with immunotherapy for advanced renal cell carcinoma and urothelial carcinoma: rationale and clinical evidence. Mol Cancer Ther 2019;18:2185–93.
19. Choueiri TK, Powles T, Burotto M, Escudier B, Bourlon MT, Zurawski B, et al. Nivolumab plus cabozantinib versus sunitinib for advanced renal-cell carcinoma. N Engl J Med 2021;384:829–41.
20. Pal S, Tsao C-K, Suarez C, Kelly W, Pagliaro L, Vaishampayan U, et al. Cabozantinib in combination with atezolizumab as first-line therapy for advanced clear-cell renal cell carcinoma: results from the COSMIC-021 study. Ann Oncol 2020;31:S554.
21. Kelley RK, Yau T, Cheng A-L, Kaseb A, Qin S, Zhu A, et al. Cabozantinib plus atezolizumab versus sorafenib as first-line systemic treatment for advanced hepatocellular carcinoma: results from the randomized phase 3 COSMIC-312 trial. Ann Oncol 2022;33:114–6.
22. Bannen LC, Bui M, Jiang F, Wang Y, Xu W. WO2019148044A1 - Compounds for the treatment of kinase-dependent disorders; 2019. Available from: https://patentimages.storage.googleapis.com/f6/cc/c1/ca4d101aad5ffa/WO2019148044A1.pdf.
23. Li B, Torossian A, Sun Y, Du R, Dicker AP, Lu B. Higher levels of c-Met expression and phosphorylation identify cell lines with increased sensitivity to AMG-458, a novel selective c-Met inhibitor with radiosensitizing effects. Int J Radiat Oncol Biol Phys 2012;84:e525–31.
24. Egile C, Kenigsberg M, Delaisi C, Begassat F, Do-Vale V, Mestadier J, et al. The selective intravenous inhibitor of the MET tyrosine kinase SAR125844 inhibits tumor growth in MET-amplified cancer. Mol Cancer Ther 2015;14:384–94.
25. Asaoka Y, Tada M, Ikenoue T, Seto M, Imai M, Miyabayashi K, et al. Gastric cancer cell line Hs746T harbors a splice site mutation of c-Met causing juxtamembrane domain deletion. Biochem Biophys Res Commun 2010;394:1042–6.
26. Eklund L, Bry M, Alitalo K. Mouse models for studying angiogenesis and lymphangiogenesis in cancer. Mol Oncol 2013;7:259–82.
27. Cheng Y, Prusoff WH. Relationship between the inhibition constant (K_I) and the concentration of inhibitor which causes 50 percent inhibition (I_{50}) of an enzymatic reaction. Biochem Pharmacol 1973;22:3099–108.
28. Smolen GA, Sordella R, Muir B, Mohapatra G, Barmettler A, Archibald H, et al. Amplification of MET may identify a subset of cancers with extreme sensitivity to the selective tyrosine kinase inhibitor PHA-665752. Proc Natl Acad Sci U S A 2006;103:2316–21.
29. Rothlin CV, Ghosh S, Zuniga EI, Oldstone MB, Lemke G. TAM receptors are pleiotropic inhibitors of the innate immune response. Cell 2007;131:1124–36.
30. Paolino M, Choidas A, Wallner S, Pranjic B, Uribesalgo I, Loeser S, et al. The E3 ligase Cbl-b and TAM receptors regulate cancer metastasis via natural killer cells. Nature 2014;507:508–12.
31. Zhou J, Tang Z, Gao S, Li C, Feng Y, Zhou X. Tumor-associated macrophages: recent insights and therapies. Front Oncol 2020;10:188.
32. Myers KV, Amend SR, Pienta KJ. Targeting Tyro3, Axl and MerTK (TAM receptors): implications for macrophages in the tumor microenvironment. Mol Cancer 2019;18:94.
33. Goel HL, Mercurio AM. VEGF targets the tumour cell. Nat Rev Cancer 2013;13:871–82.
34. Shojaei F, Lee JH, Simmons BH, Wong A, Esparza CO, Plumlee PA, et al. HGF/c-Met acts as an alternative angiogenic pathway in sunitinib-resistant tumors. Cancer Res 2010;70:10090–100.
35. Elisei R, Schlumberger MJ, Muller SP, Schoffski P, Brose MS, Shah MH, et al. Cabozantinib in progressive medullary thyroid cancer. J Clin Oncol 2013;31:3639–46.
36. Brose MS, Robinson B, Sherman SI, Krajewska J, Lin CC, Vaisman F, et al. Cabozantinib for radioiodine-refractory differentiated thyroid cancer (COSMIC-311): a randomised, double-blind, placebo-controlled, phase 3 trial. Lancet Oncol 2021;22:1126–38.
37. Choueiri TK, Escudier B, Powles T, Tannir NM, Mainwaring PN, Rini BI, et al. Cabozantinib versus everolimus in advanced renal cell carcinoma (METEOR):

final results from a randomised, open-label, phase 3 trial. Lancet Oncol 2016;17:917–27.
38. Choueiri TK, Halabi S, Sanford BL, Hahn O, Michaelson MD, Walsh MK, et al. Cabozantinib versus sunitinib as initial targeted therapy for patients with metastatic renal cell carcinoma of poor or intermediate risk: the Alliance A031203 CABOSUN trial. J Clin Oncol 2017;35:591–7.
39. Abou-Alfa GK, Meyer T, Cheng AL, El-Khoueiry AB, Rimassa L, Ryoo BY, et al. Cabozantinib in patients with advanced and progressing hepatocellular carcinoma. N Engl J Med 2018;379:54–63.
40. Lacy SA, Miles DR, Nguyen LT. Clinical pharmacokinetics and pharmacodynamics of cabozantinib. Clin Pharmacokinet 2017;56:477–91.
41. Hsu J, Chong C, Goon L, Balayan J, Wu S, Johnson E, et al. XL092, a multi-targeted inhibitor of MET, VEGFR2, AXL and MER with an optimized pharmacokinetic profile. Eur J Cancer 2020;138:S16.
42. Lin Y, Xu J, Lan H. Tumor-associated macrophages in tumor metastasis: biological roles and clinical therapeutic applications. J Hematol Oncol 2019;12:76.
43. Corliss BA, Azimi MS, Munson JM, Peirce SM, Murfee WL. Macrophages: an inflammatory link between angiogenesis and lymphangiogenesis. Microcirculation 2016;23:95–121.
44. De Palma M, Biziato D, Petrova TV. Microenvironmental regulation of tumour angiogenesis. Nat Rev Cancer 2017;17:457–74.